

# Antenna-Range Consistency in Measurements of Gain and Phase Patterns

George Purcell,\* Larry Young,\* and Luis Zuniga\*

**ABSTRACT.** — Measurements have been conducted at two antenna ranges to assess whether internal range errors allow determination of the electrical location (phase center) of a Global Positioning System receiving antenna with submillimeter accuracy in the 1.1–1.6 GHz band. We first measured antennas in the tapered far-field chamber at Goddard Space Flight Center and later duplicated some of those measurements in the spherical near-field chamber at Nearfield Systems, Inc. (NSI).

In general, the two ranges perform about equally well. Position errors due to thermal noise, mounting uncertainty, and instrumental drift are negligible at both. Multipath power at Goddard is about 40 dB below the direct signal but could significantly corrupt measurements at boresight angles near 90 deg. At NSI, multipath is about 50 dB below the direct signal after the application of software that detects it and reduces the effect.

Direct comparison of phase centers calculated for identical configurations at the two ranges gives consistent results with a standard deviation of 0.58 mm. However, an offset of 6.5 mm remains unexplained. More detailed comparison of antenna phases over a range of directions also shows submillimeter consistency.

## I. Background

The proposed Geodetic Reference Antenna in Space (GRASP) mission [1] undertakes to improve the definition of the Terrestrial Reference Frame (TRF) by making precise collocated measurements of the four space geodetic techniques that contribute to the TRF: global navigation satellite systems (GNSSs), very long baseline interferometry (VLBI), satellite laser ranging (SLR), and Doppler orbitography and radiopositioning integrated by satellite (DORIS). In order to relate the four techniques with the required accuracy of 1 mm, it is necessary know the positions of all the sensors, relative to each other and to the center of mass of the spacecraft, with even smaller uncertainty. These positions are generally a combination of several mechanical offsets plus the offset of the effective electrical or optical

---

\* Tracking Systems and Applications Section.

The research described in this publication was carried out by the Jet Propulsion Laboratory, California Institute of Technology, under a contract with the National Aeronautics and Space Administration. © 2015 California Institute of Technology. U.S. Government sponsorship acknowledged.

location of the sensor relative to a reference location that typically is at an easily accessible place on the physical structure of the sensor. Each of these components contributes to the total error in the location of the sensor, but in this article we are concerned only with the final piece: the sensor’s effective location in the sensor coordinate frame.

For the radio-frequency sensors, the position of the sensor is determined by measurements at an antenna test range of the effective location (“phase center”) of the antenna relative to a fiducial point on the antenna structure. In general, the “effective location” — the place where the antenna seems to “be” for an incoming signal — varies with the direction of the incoming signal in the antenna’s field of view, but for any specified field of view there is a particular location that minimizes the RMS distance between the actual phase center and that location, and that is what we refer to here as the phase center.

Calculation of the location of the phase center relies on phase measurements made at the range. In order to judge the accuracy of the phase center, then, we need to understand all the components that contribute to errors in the measured phase pattern, and how those errors affect the computation of the phase center. Elaborate models such as the 18-component National Institute of Standards and Technology (NIST) model [2] for planar near-field ranges, and its variants, have been constructed and used to evaluate specific ranges.<sup>1</sup> However, these range surveys are time-consuming and expensive; and there is always a question whether a survey, done at some time in the past, where components of the error budget have been painstakingly isolated and evaluated under tightly controlled conditions, truly applies to the current measurements. This concern is particularly apropos when the required accuracy of the measurements is comparable to the range’s ultimate capability, as it is in our case.

We have therefore adopted the more heuristic, user-centered approach of comparing repeated measurements of a single antenna similar to the one that GRASP will use for GNSS signals: measurements repeated in time, repeated with different configurations, and repeated at different kinds of range. For the investigation reported here, we measured our antenna first at a tapered far-field range, the Goddard Electromagnetic Anechoic Chamber (GEAC) at the Goddard Space Flight Center in Greenbelt, Maryland, and then again in the spherical near-field chamber of the Allen C. Newell Near-Field Antenna Measurement Facility at Nearfield Systems, Incorporated (NSI), in Torrance, California.

Certainly this method has disadvantages. Repetitions do not detect static errors at a single range, and fluctuations may be hard to identify with a specific source. If two ranges behave differently, it may be hard to associate that behavior with a specific source. Still, some error sources have identifiable signatures, and if results at different ranges agree at the desired level, we are entitled to limited confidence that those results are accurate at that same level. The following two sections describe the measurements that we made and our interpretation of the results.

---

<sup>1</sup> For example, Allen C. Newell, “Range Assessment Report: NSI Near-Field Antenna Range,” Nearfield Systems, Incorporated, August 14, 2007.

## II. Measurements

A note on terminology: In what follows we will use the word “measurement” in a generic sense and in particular to refer to a single antenna gain or phase value in a particular direction. A series of measurements made consecutively that constitute a complete antenna pattern will be called a “scan.”

### A. Strategy

As explained above, as ordinary users making our pattern measurements according to the ranges’ standard protocols, we are limited in what we can do to isolate and evaluate individual elements of the error budget. Nevertheless, there are things we can do by making the same measurement in different ways that do expose range errors. Here are some errors to which our data are sensitive:

(1) *Random errors.* If we repeat a scan exactly, even in the absence of instrumental drift the results will differ slightly because of noise in the data. We cannot eliminate drift between two scans, but we can see noise within a scan by fitting a smooth curve to a limited number of contiguous points that should vary slowly and smoothly, and calculating the RMS residual to the fit. Rounding error also contributes to this residual. However, both gains (in dB) and phases (in degrees) are reported to us with three decimal places, and rounding error contributes negligibly to the total RMS error. For our calculations, we fitted cubic polynomials to a series of 11 points (7 degrees of freedom).

A second way to estimate random noise is to perform a scan and then repeat it as exactly as possible. We can then calculate the RMS difference between the two measurements and divide by  $\sqrt{2}$  to get the standard deviation of an undifferenced measurement. This approach is sensitive to errors that do not affect the curve-fitting method, like instrumental drift and failure to reproduce the orientation of the antenna exactly; but the drift, at least, can be virtually eliminated by removing a low-order polynomial fit from the differenced time series before calculating the RMS. We found that a linear polynomial was sufficient in all cases.

(2) *Mechanical alignment.* If the antenna under test (AUT) is mounted on the positioner — or on the GRASP spacecraft — several times, its position relative to the surrounding structure may vary because of play in the mounting hardware. Generally the hardware is made to fit snugly and is tightened consistently so that the play is negligible, but when submillimeter precision is needed it is prudent to determine at least an upper bound on the variability. We did that in one case by performing a scan, then loosening and retightening the mounting bolts, and scanning again. In two other cases, we dismounted the AUT entirely, made unrelated measurements, and later remounted and rescanned.

(3) *Instrumental drift.* Circumstances such as changes in the temperature of electronic components and cables can cause the reported gain and phase to change from one scan to another and even within a single scan. Because GRASP is interested primarily in the phase center, gain changes are of little concern; and a constant phase offset between scans does not affect the phase center, because the phase-center calculation depends only of the variation of phase over the antenna’s field of view. However, drift within a scan does affect the reported phase pattern.

At a far-field chamber like GEAC, there is an easy way to monitor instrumental drift on a fairly short time scale. Over the course of a scan, one particular point in the pattern, the boresight direction, is observed repeatedly at regular intervals. If the boresight phase varies systematically, then either (a) the instrumental phase is drifting, or (b) the range reference (receiving) antenna is combining orthogonal linear polarizations imperfectly to get right-circular polarization (RCP). However, (b) imposes a characteristic signature on the pattern of variation, so (a) and (b) are usually distinguishable. If drift is present, we then have to ask how it affects the phase center and whether it is possible and necessary to reduce its effect.

At a near-field chamber like the one at NSI (see Section II.D below), the measurements are processed as spherical harmonics and then converted to angular coordinates for output, so that instrumental drift, if it exists, is smoothed over the entire scan and made undetectable.

(4) *Chamber multipath.* Chamber multipath is reflections of the test signal from surfaces and edges in the chamber or on its walls that interfere with the direct signal at the reference antenna and thereby corrupt the pattern measurements. Of course, layers of absorber throughout the chamber suppress most reflection. Moreover, specular reflection reverses the sense of circular polarization, which tends to decrease the effect further for RCP antennas like ours. On the other hand, the absorber is not perfect, the actual reflection or scattering is not generally specular, and interference is more of a problem when the direct signal probes the low-gain outer part of the beam while the multipath comes in near the boresight. As a result, multipath may well be the dominant source of range error.

In our measurements, we detected multipath in two ways. First, the way the antenna pattern is sampled at far-field ranges like GEAC lets us measure a particular point in the pattern (other than the boresight axis) with the boresight pointing in two different directions. If the angle between those directions is large, as it is for measurements far from the boresight, then the difference between the two measurements tells us something about the magnitude of multipath, although it does not tell much about the location of the source. A shortcoming of this method is that it is sensitive only to asymmetry in the multipath signal between the left and right sides of the chamber. Section III.B explains this method in detail.

Our other approach to multipath relies largely on the measurements made in the near-field chamber at NSI. There, software called Mathematical Absorber Reflection Suppression (MARS) works to detect and reduce the effects of whatever multipath is present [3]. We can then compare the patterns before and after MARS to see what MARS thinks the multipath environment is at NSI, and we can compare the (presumably multipath-free) patterns with MARS to those obtained at GEAC to get an idea of the multipath at GEAC.

(5) *Other chamber errors.* The errors listed above are only the easily observed subset of the full list of possibilities. Some of the other errors will be negligible. Others will alias to some extent into the ones observed. For example, random errors in the reported angles will look like random noise; polarization mismatch in the reference antenna will resemble instrumental drift. Still other errors, like miscalibration of reference-antenna gain and curvature of the far-field wavefront, are undetectable at the range where they occur but do affect a

comparison between patterns at different ranges. We hope that we can at least show that the dominant error sources are small enough to allow GRASP to meet its sensor-location requirements.

The remaining subsections give more information about the details of our three measurement sessions.

#### **B. Session 1: Measurements at GEAC, January 2014**

Our first group of measurements took place at GEAC on January 27, 2014. We used the tapered far-field chamber, where the distance between the AUT, which transmits, and the receiving antenna is about 16.8 m. Our test antenna was an Exelis (formerly Dorne & Margolin) model C146-27-1 mounted on a lightweight two-ring choke. Its gain on boresight is 7–8 dBiC at GNSS frequencies, and it will be used out to boresight angles of 75–90 deg as a precision orbit determination (POD) antenna on the Constellation Observing System for Meteorology, Ionosphere, and Climate–2 (COSMIC-2) spacecraft constellation. In the chamber, the antenna was attached to a cylindrical cage that allows access to the back of the antenna for electrical connections; then the cage was mounted on the positioner itself, as shown in Figure 1.

To sample the antenna pattern over the sphere, the positioner rotates the antenna around two axes in the standard way for ranges of this kind. First, the operator positions the antenna on the horizontal head-angle axis, which is nominally the axis of circular symmetry of the POD antenna in Figure 1. In this article, we call the positioner’s orientation on the head-angle axis  $\phi$  by analogy with ordinary spherical coordinates, and the antenna is mounted so that a specific point on the antenna has a particular orientation at  $\phi = 0$  deg. In this way,  $\phi$  can refer to directions on the antenna itself as well as the positioner. When the antenna rotates clockwise, as seen from the receiving antenna,  $\phi$  increases.

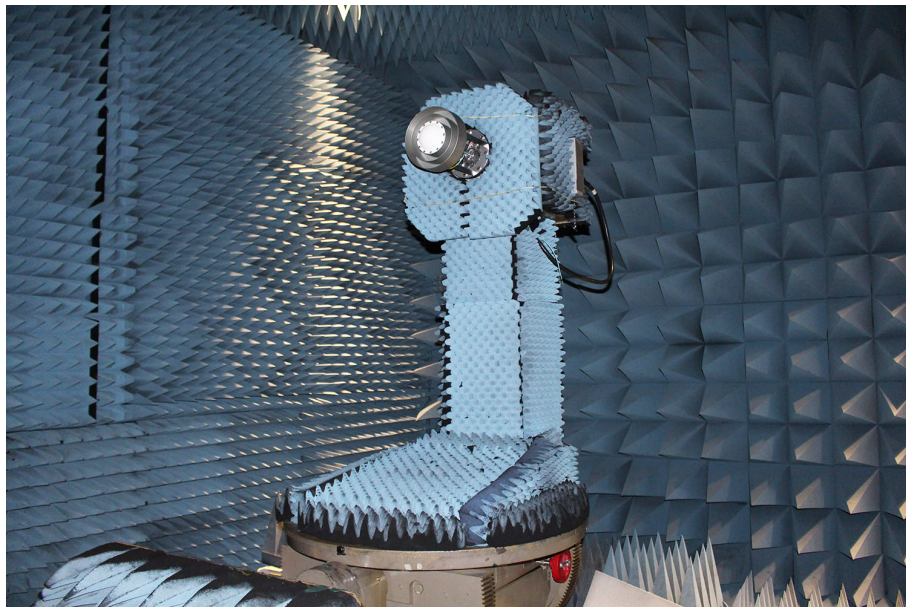


**Figure 1. Exelis antenna and two-ring choke mounted in the Goddard far-field chamber.**

Having set  $\phi$ , the operator rotates the upper part of the positioner, and thereby the antenna, around the vertical azimuth axis, which is the axis of the turntable visible just above the red crank in Figure 1. (This nomenclature is a little confusing, because when an antenna like the POD antenna in the figure is mounted on the ground with its beam pointing up, motion around the positioner's azimuth axis corresponds to changes in terrestrial elevation, and motion around the head-angle axis corresponds to changes in terrestrial azimuth.) In this article, we call the positioner's orientation on its azimuth axis  $\theta$ , completing the analogy with spherical coordinates. When  $\theta = 0$  deg, the antenna under test directly faces the receiver, as shown in the figure, and as the turntable rotates clockwise, as seen from above,  $\theta$  increases.

To run a pattern, the operator sets  $\phi$  to  $0^\circ$  and  $\theta$  to near  $-180$  deg; that is, rotates the positioner counterclockwise as seen from above until the AUT faces directly away from the receiving antenna. Then gain and phase data are collected at the designated frequencies as the antenna scans in  $\theta$  to near  $+180$  deg. Next,  $\phi$  increases by a specified increment,  $\Delta\phi$ , and the azimuth scan is repeated. This process generally continues until  $\phi$  reaches  $180$  deg; at that point the patterns have been measured over the entire sphere. Notice that the boresight direction ( $\theta = 0$  deg) is measured for each head angle, providing a way to monitor instrumental drift. Furthermore, the azimuth scan at  $\phi = 180$  deg repeats the series of points measured at  $\phi = 0$  deg, but in the opposite direction and with the boresight direction different for corresponding points. Comparing these two series gives information about chamber multipath, and if the sequence of head angles continues from  $180$  deg through  $360$  deg, then we have two complete independent pattern measurements of the entire sphere with different orientations of the antenna at each point.

In Session 1, we measured  $\phi$  from  $0$  deg through  $180$  deg with  $\Delta\phi = 10$  deg, and  $\theta$  was reported at  $1$ -deg intervals from  $-176$  deg through  $+176$  deg for a total of  $19 \times 353 = 6707$  points per pattern. The range gave us patterns in the GPS bands centered at  $1.17645$  GHz (L5),  $1.22760$  GHz (L2), and  $1.57542$  GHz (L1) for both RCP and left-circular polarization (LCP). We also measured patterns at other frequencies, but for the analysis reported here we used only the three GPS frequencies and RCP (the nominal polarization of the GPS signals).

There were just three scans in Session 1 that bear on this article. The first scan, Trial 1, covered the entire sphere as described above. Trial 2 immediately followed Trial 1 but measured only  $\phi = 0$  deg. After Trial 2, the bolts holding the antenna against the mounting bracket were loosened and retightened, and Trial 3 repeated Trial 2 exactly. Together, the three trials enable us to estimate random noise and examine instrumental drift. The azimuth scans at  $\phi = 0$  deg and  $180$  deg in Trial 1 also give information about chamber multipath.

### C. Session 2: Measurements at GEAC, November 2014

During the week of November 17, 2014, we returned to GEAC with a number of antennas to be used on the Gravity Recovery and Climate Experiment Follow-On (GRACE-FO) spacecraft. These antennas included another Exelis model C146-27-1 antenna, which we used for the measurements relevant to GRASP. This antenna was mounted on a lightweight three-ring choke (slightly different from the two-ring choke used in Session 1), as shown

in Figure 2. We measured the antenna-plus-choke by itself (Configuration 1) and also while it was mounted on a mockup of the upper part of the GRACE Follow-on spacecraft, seen in Figure 3. Our aluminum mockup consists of an upper rectangular surface about 1.2 m long and 0.7 m wide flanked by two oblique wings. The upper surface has a circular hole in the center for the antenna-plus-choke and a trapezoidal hole modeling the well for a star tracker. When the antenna is mounted on the mockup, the upper surface of the choke (and hence the lower surface of the antenna proper) is just about coplanar with the mockup. We measured patterns for the antenna both with the star-tracker well completely covered by copper tape (Configuration 2), and with the well open (Configuration 3) as shown in Figure 3. Although we did succeed in repeating some measurements, two different attempts to probe chamber multipath failed because it was masked by multipath from the mockup.

#### **D. Session 3: Measurements at Nearfield Systems, Inc., March 26, 2015**

At NSI we used the Model 700S-75 spherical near-field measurement system in the Allen C. Newell Near-Field Antenna Measurement Facility. Figure 4 is a drawing of the positioner of this system, and Figure 5 shows our C146-27-1 antenna and three-ring choke mounted in the chamber. Although the rotations of the AUT in this chamber are basically the same as those at GEAC, the chamber is different, and the processing of the near-field data is entirely different; so measuring here allowed us to repeat the GRASP measurements from Session 2 and compare the results to see how well they agree.

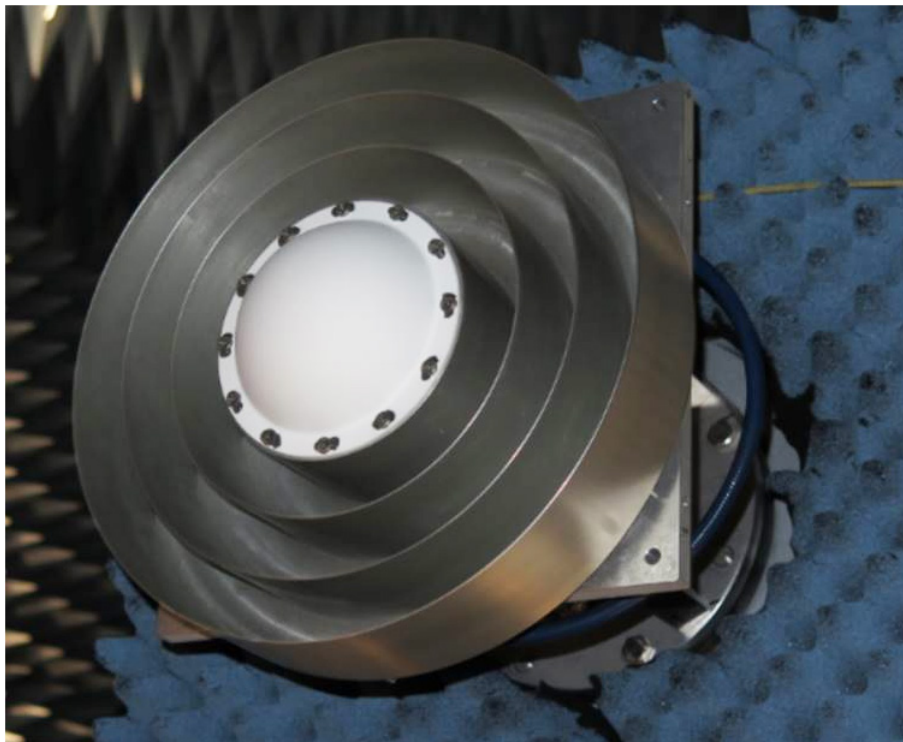


**Figure 2. Exelis antenna and three-ring choke mounted in the Goddard far-field chamber.**

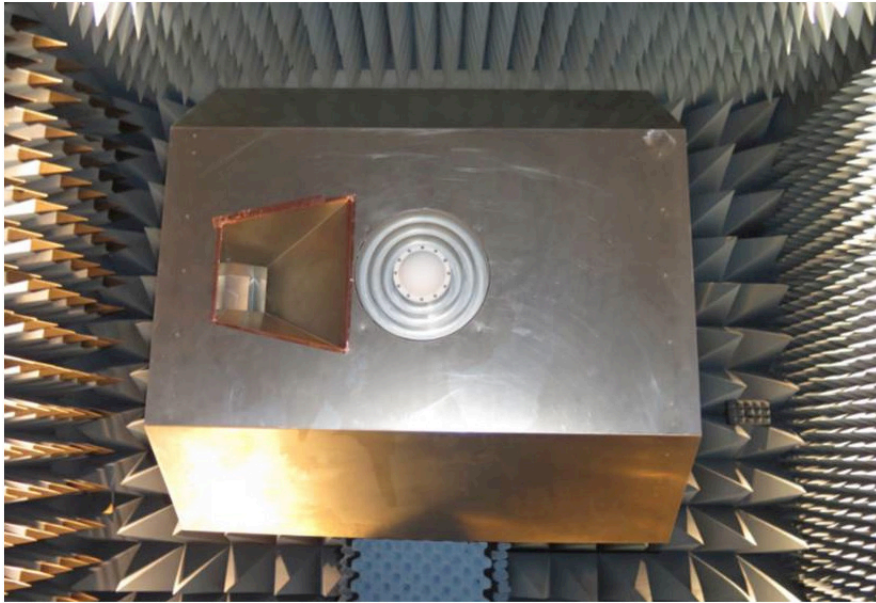


Figure 3. Antenna mounted with mockup of the GRACE Follow-On spacecraft at Goddard.

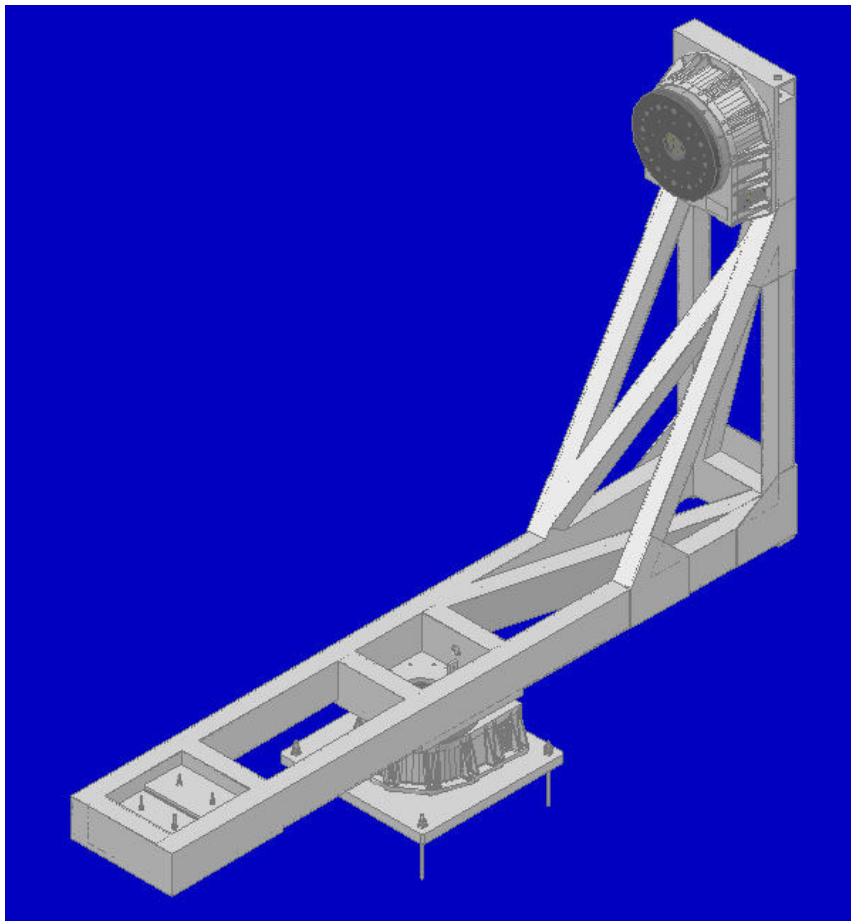
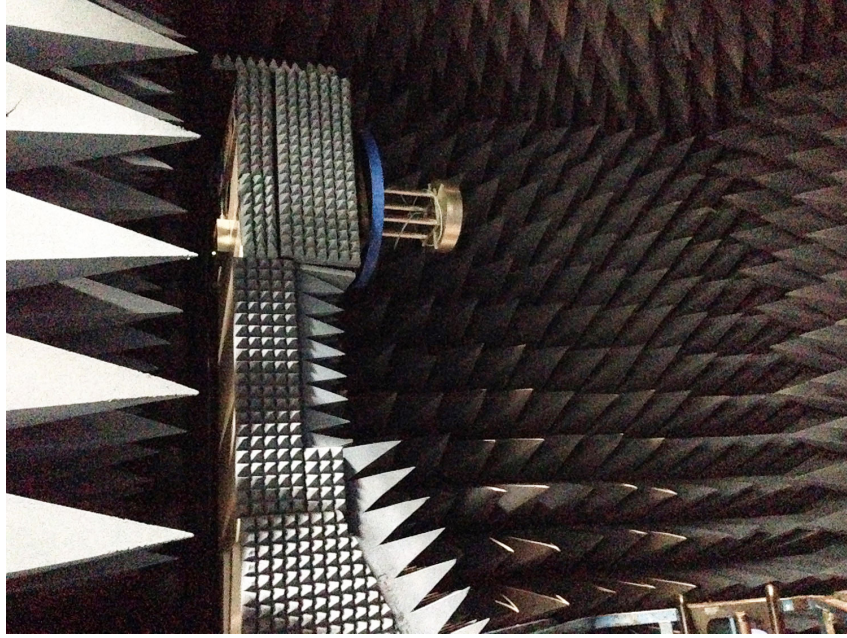


Figure 4. Antenna positioner of the Model 700S-75 near-field measurement system at NSI.



**Figure 5. Antenna mounted in the NSI spherical near-field chamber.**

Our program was first to repeat the GEAC measurement of Configuration 1 (Scan 1), then redo Configuration 2 (Scan 2), then Configuration 3 (Scan 3), and finally reprise Scan 1 to check repeatability (Scan 4). The range and resolution of the measurements did differ slightly from Session 2. For purposes of comparison, we generally used the intersection of the two data sets:  $\theta$  from  $-179$  deg through  $+179$  deg at 1-deg increments,  $\phi$  from 0 deg through 180 deg at 10-deg increments, and the center frequencies of the GPS L1, L2, and L5 bands.

As mentioned above in Section II.A, NSI also provides MARS software to reduce the effect of chamber multipath. We have pattern measurements both before and after the MARS adjustments and have examined their effect on the NSI data as well as what they may reveal about multipath at GEAC.

### **III. Results**

This section presents our results for random errors, mounting repeatability, instrumental drift, and chamber multipath.

#### **A. Random Errors and Instrumental Drift**

Random noise in this context should mostly be thermal noise on the electrical signals being measured. We expect it to have a nearly Gaussian distribution, to be statistically independent at all measurement points, and to affect gain and phase measurements in basically the same way. There is a small contribution to random noise from round-off error, but since gain (in dB) and phase (in degrees) are reported to three decimal places, that component

should be negligible. There could also be a tiny superficially random contribution from failure to measure at exactly the reported values of  $\theta$  and  $\phi$ , but that component is probably biased and highly correlated.

We estimated random noise in two ways: first by fitting a cubic polynomial to 11-point sequences of adjacent data points, and second by attempting to repeat a measurement exactly.

#### 1. Estimates of random errors from cubic least-squares fits

In Session 1, we fitted cubic polynomials to both gain and phase data from our POD antenna at L1, L2, and L5,  $\phi = 0$  deg, and intervals in  $\theta$  of  $-5$  deg through  $+5$  deg,  $15$  deg through  $25$  deg, and  $35$  deg through  $45$  deg. Then we calculated an RMS residual, accounting for the correct number of degrees of freedom:

$$D = \left[ \frac{\sum_{i=1}^n (m_i - P_i)^2}{n - n_p} \right]^{1/2}, \quad (1)$$

where

- $D$  is the RMS scatter of the measurements relative to the polynomial, accounting for the correct number of degrees of freedom, in the same units as the measurements,
- $n$  is the number of measurements, in this case  $33 = (3 \text{ sets of points}) \times (11 \text{ points per set})$ ,
- $m_i$  is the  $i$ -th measurement, whether gain or phase,
- $P_i$  is the value of the appropriate cubic polynomial (fitted by least squares to a series of 11 points), evaluated at the argument of  $m_i$ , and
- $n_p$  is the number of fitted parameters, in this case  $12 = (4 \text{ coefficients per cubic polynomial}) \times (3 \text{ polynomials})$ .

$D$  can then be converted to a voltage signal-to-noise ratio  $\Sigma_V$ . For gains in dB,

$$\Sigma_V = (10^{D/20} - 1)^{-1}, \quad (2a)$$

and for phases in degrees,

$$\Sigma_V = (D\pi/180)^{-1}. \quad (2b)$$

Table 1 gives the results.

Certainly these residuals are insignificant relative to GRASP's requirements, and it would be surprising if they were not, since this is a very manageable error source. The agreement of the SNRs derived from the gain and phase measurements, at least at L5 and L2, gives us confidence that we basically understand what is going on here. As expected, the contribution of round-off error, an RMS of  $0.001/\sqrt{12} = 0.00029$  (in units of either dB or degrees) is negligible.

**Table 1. Gain and phase residuals from Session 1 with calculated SNRs.**

Frequency Band	RMS Gain Residual, dB	$\Sigma_V$ , Voltage SNR from Scatter of Gains	RMS Phase Residual, deg	RMS Phase Residual, mm	$\Sigma_V$ , Voltage SNR from Scatter of Phases
L5	0.004207	2064	0.03000	0.02123	1910
L2	0.004500	1930	0.03058	0.02074	1874
L1	0.003732	2327	0.01441	0.00762	3976

We analyzed data from Session 2 in the same way, this time using data from the second POD antenna and choke ring described in Section II.C. Table 2 gives the results.

**Table 2. Estimated random noise in gain and phase from Session 2 with calculated SNRs.**

Frequency Band	RMS Gain Residual, dB	$\Sigma_V$ , Voltage SNR from Scatter of Gains	RMS Phase Residual, deg	RMS Phase Residual, mm	$\Sigma_V$ , Voltage SNR from Scatter of Phases
L5	0.008212	1057	0.10164	0.07195	564
L2	0.008279	1049	0.06330	0.04294	905
L1	0.003354	2589	0.05890	0.03114	973

These numbers differ significantly from those in Table 1: The L2 and L5 gain residuals are about twice as large, and the SNRs inferred from gain and phase no longer agree even approximately. We have no explanation for this behavior; nevertheless, the phase errors in millimeters are still insignificant relative to GRASP's requirements.

## 2. Estimates of random errors and instrumental drift from repeated measurements.

We can estimate random errors in a second way by making the measurements twice and comparing the results. This approach differs from the first in that it is subject to errors that are not strictly random. For example, instrumental drift can occur between the scans, and as the interval between scans increases, we can expect the drift to accumulate. Also, if the antenna is dismounted between the scans, then it is possible that it may be remounted in a slightly different location, which will affect at least the phase measurements. Hence, by repeating scans under various circumstances and comparing the results among themselves and with the results of curve fitting we can get an idea of some additional effects that can cause phase-center estimates to differ.

In Session 1, we performed the three trials described above in Section II.B. Figure 6 shows the series of phases measured at the three GPS frequencies during Trial 1, in the boresight direction ( $\theta = 0$  deg), for sequential values of  $\phi$ . A constant has been added to each series to make the mean value zero for easier comparison. The figure also shows a quadratic fit to each series, with the coefficients displayed for quantitative comparison.

Systematic variation of the kind seen here must be the result of either instrumental drift or an imperfect combination of linear polarizations to give RCP and LCP. However, the latter has a distinctive sinusoidal signature with a period of 180 deg in  $\phi$  that does not appear here, so what we see in the figure must be genuine drift. It is interesting that the drift rate is about the same at all three frequencies (that is, it does not scale with frequency), and it is changing at a fairly constant rate throughout the scan. Using the polynomial fit to L5 for calculation, we find that the change in instrumental phase over the length of the

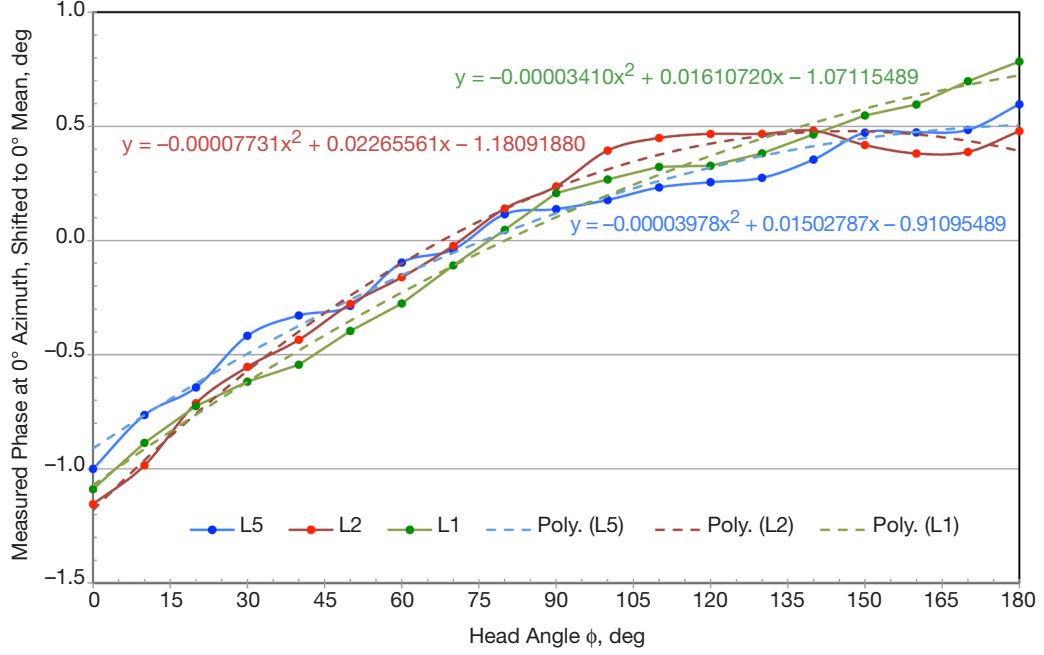


Figure 6. Instrumental drift and polynomial fits at 0 deg azimuth.

scan (about 9 min) is  $0.505 \text{ deg} - (-0.911 \text{ deg}) = 1.416 \text{ deg}$ , and the change in phase rate is  $2 \times (-0.00003978) \times 180^2 = 2.578 \text{ deg/scan}$ . Additional analysis of Trials 2 and 3, not shown here, indicates that this drift in phase rate continues at about the same level during those measurements.

The issue for GRASP, then, is what effect a drift at this level has on the solved phase center. To answer this question, we compared phase center solutions for Trial 1 calculated in two ways at the three frequencies. First, we used the phase measurements just as they were given to us, and second we forcibly removed the apparent drift by subtracting from the raw data the polynomials shown in Figure 6. Table 3 shows the comparison in terms of the parameters of the phase-center fit.

Table 3. Differences between phase-center solutions with and without measurement drift.

	L1	L2	L5
$\Delta \zeta_0$ , mm	-0.5448	-0.7860	-0.6248
$\Delta d$ , mm	0.0001	-0.0003	-0.0001
$\Delta r$ , mm	-0.0009	-0.0104	-0.0050
Raw RMS residual, deg	2.9888	1.1616	1.1694
Detrended RMS residual, deg	2.9581	1.0172	1.0540

The phase-center model is described in more detail below in Section III.C. In Table 3,  $\zeta_0$  is a phase constant not directly related to the phase-center location,  $d$  specifies the location of the phase center along the  $\phi$  axis,  $r$  is the distance from the phase center to the  $\phi$  axis, and the residuals are the difference between the observed and model phases. The table shows that the change ( $\Delta$ ) in the estimated phase-center location caused by instrumental drift, at

least in this case, is negligible (relative to the GRASP requirement) in the parameters that specify the actual location of the phase center. The global phase constant absorbs most of the effect, and the residuals improve about 8 percent on the average.

In order to calculate a statistic from repeated data that better reproduces the random noise calculated from polynomial fits (Section 2.A.1), we can remove the effect of drift by differencing our two data sets and then subtracting a fitted offset and slope from the difference, just as we did above for Trial 1. Finally, we have to divide the RMS of the resulting sequence by  $\sqrt{2}$  to get the equivalent RMS for a single data set. We did this calculation for both gains and phases in Trials 1 and 2, using only  $\phi = 0$  deg (since that is all we had for Trial 2) and  $\theta$ s from  $-40$  deg through  $+40$  deg. Table 4 gives those results.

**Table 4. Estimated random noise from differenced data with drift removed, Session 1.**

Frequency Band	RMS Gain Residual, dB	$\Sigma_V$ , Voltage SNR from Scatter in Gains	RMS Phase Residual, deg	RMS Phase Residual, mm	$\Sigma_V$ , Voltage SNR from Scatter in Phases
L5	0.005652	1536	0.03672	0.02599	1560
L2	0.003976	2184	0.02817	0.01911	2034
L1	0.002706	3210	0.01328	0.00702	4316

These values are consistent with those in Table 1, indicating that we have done an adequate job of removing the drift. However, we need to be circumspect in interpreting RMS residuals in terms of SNRs for repeated measurements, because those residuals can contain systematic (correlated) behavior caused by slight differences in the circumstances of the measurements.

As mentioned above, we used Trial 3 to check whether loosening and retightening the AUT's mounting bolts (essentially remounting the antenna) would affect the measurements perceptibly. To that end, we formed differenced phases with linear drift removed for Trial 3 relative to Trials 1 and 2, exactly as described above for Trial 2 relative to Trial 1, and compared the RMS residuals for all three differences at the three frequencies. The residuals for the differences involving Trial 3 are slightly higher than those for Trial 2 relative to Trial 1, but the difference is not statistically significant (passes the F test for equality of the variances at the 35 percent level). As expected, mounting variability is apparently not a significant component of the chamber error budget at the level relevant to GRASP.

Using data from Session 2, we followed the same procedure to compare two nominally identical data sets. In this case, the AUT included the GRACE-FO mockup, and we used data from  $\theta = 40$  deg through  $0$  deg and  $\phi = 0$  deg through  $170$  deg. Most significantly, for the comparison the AUT was removed from the positioner and other measurements were performed before we remounted the original AUT for the second scan. Table 5 gives those results.

These numbers are roughly comparable with Table 2, and they show much better consistency among the frequencies. Like Table 2, they show greater noise than Session 1, but here we have a probable explanation: A few values of head angle show conspicuous oscillations in the differenced gain and phase that apparently result from slight differences in mul-

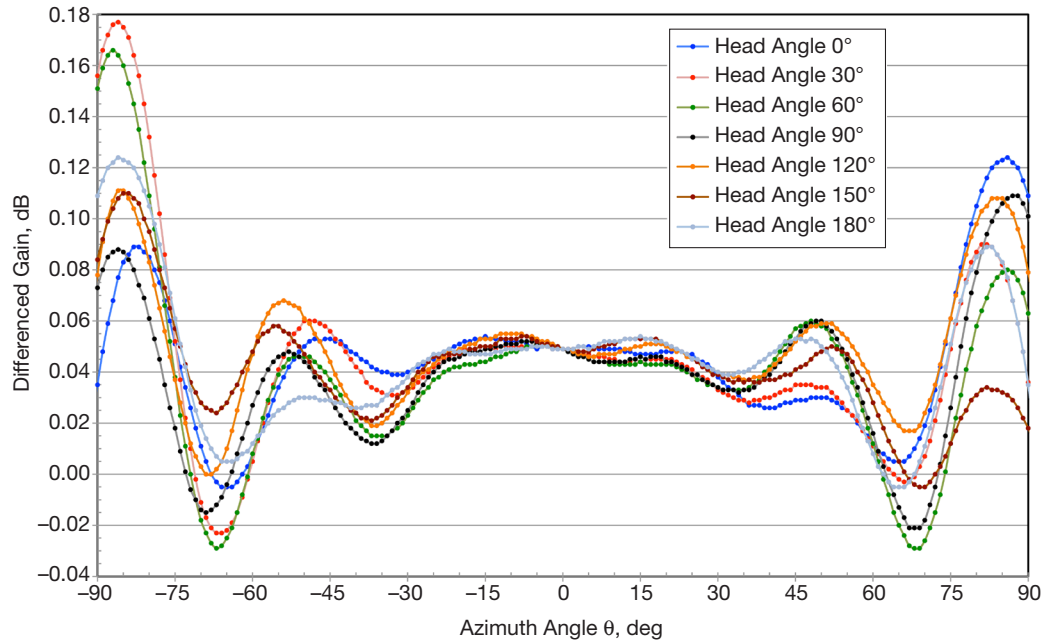
**Table 5. Estimated random noise from differenced data with drift removed, Session 2.**

Frequency Band	RMS Gain Residual, dB	RMS Phase Residual, deg	RMS Phase Residual, mm
L5	0.01049	0.08161	0.05777
L2	0.00969	0.06727	0.04564
L1	0.01023	0.09531	0.05038

tipath from the edges of the mockup. Those differences probably arise because the mockup is mounted slightly differently during the two scans that are being compared. Because of these oscillations, it is no longer possible to treat the variance as entirely random and interpret it in terms of SNR.

If we had been able to compare measurements of the antenna without the mockup, the differences between the two scans would probably have been significantly smaller. But even at the level observed, the measurement uncertainties pose no threat to GRASP's requirements.

During Session 3, we ran Scan 4 specifically for comparison with the nominally identical Scan 1. As an example, Figure 7 shows the difference between the gains measured at the L2 frequency in the two scans for seven values of  $\phi$ . This plot is typical of NSI data, with its smooth variation looking like the difference between slightly different sums of spherical harmonics up to some moderate degree. At NSI, the effect of instrumental drift has been suppressed, so that the points at boresight angle 0 deg are all exactly the same. Also the values for  $\phi = 180$  deg are exactly, not approximately, the reverse of the values at  $\phi = 0$  deg, depriving us of our most convenient tool for detecting chamber multipath.



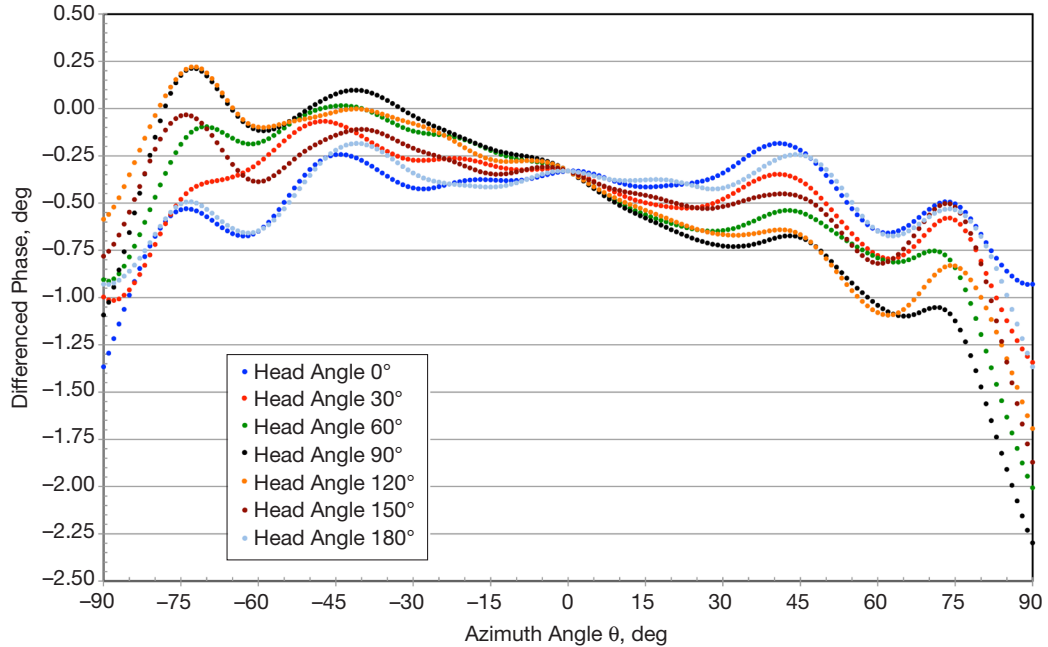
**Figure 7. Differenced gain for nominally identical scans at NSI, L2 frequency.**

Table 6 gives the gain results for Session 3 next to the results for the same antenna (but with the spacecraft mockup) from Session 2. Here again, the standard deviations of the differenced data have been divided by  $\sqrt{2}$  to give a value applicable to undifferenced data. For the NSI data, we used  $\theta$ s from  $-40$  deg through  $+40$  deg and all the  $\phi$ s from  $0$  deg through  $175$  deg. Here, the standard deviation of the differences is somewhat better at NSI than at GEAC, where the repeated measurement was apparently affected by a slight difference in the geometry of the antenna plus mockup, as mentioned above. On the other hand, there is a bias of about  $0.05$  dB at NSI (conspicuous in Figure 7) that is practically absent at GEAC. (This bias remains when the MARS adjustments are applied.)

**Table 6. Bias and standard deviation of repeated gain measurements at GEAC and NSI.**

	Bias, dB		Standard Deviation, dB	
	GEAC	NSI	GEAC	NSI
L5	-0.00913	0.05112	0.01049	0.00560
L2	-0.00045	0.04225	0.00969	0.00665
L1	0.01463	0.06236	0.01023	0.01062

Figure 8 shows the corresponding difference of the phases measured at L2 in Scans 4 and 1 at NSI. Again we see the smooth variation in  $\theta$  and systematic dependence on  $\phi$ , but there is also a surprising slope in the neighborhood of  $\theta = 0$  deg that is most prominent near  $\phi = 90$  deg and absent or slightly reversed at  $0$  deg and  $180$  deg. This behavior appears also at L5 and L1 (not shown), and it remains at about the same level after NSI's MARS adjustments, although it affects the three frequencies differently. Table 7 summarizes the statistics of the phase differences at GEAC and NSI.



**Figure 8. Differenced phase for nominally identical scans at NSI, L2 frequency.**

**Table 7. Standard deviation of repeated phase measurements at GEAC and NSI.**

	Standard Deviation, mm	
	GEAC	NSI
L5	0.08276	0.08944
L2	0.07355	0.08543
L1	0.07706	0.06559

Here, as in Table 6, the underlying data are made as much alike as possible: at GEAC,  $\theta$ s from  $-40$  deg through  $0$  deg and  $\phi$ s from  $0$  deg through  $170$  deg; at NSI,  $\theta$ s from  $-40$  deg through  $+40$  deg and  $\phi$ s from  $0$  deg through  $175$  deg. For phases, a constant bias does not affect the phase center calculation, so only the standard deviations are listed in Table 7. Although the patterns of the differences at the two ranges are quite different, the scale of the variations is very similar and not a significant source of error for GRASP.

## B. Chamber Multipath

As we began this investigation, we expected that signal multipath would dominate the chamber error budget and that random errors, instrumental drift, and misalignment would be minor or insignificant contributors. In fact, the data bear out that expectation. Because of the difference between far- and near-field ranges, we used different methods at GEAC and NSI to detect multipath, as described in the following subsections.

### 1. Multipath detection at GEAC

At Goddard, the series of azimuth angles at head angles  $0$  deg and  $180$  deg measure exactly the same points in the antenna pattern but in opposite directions. If only the direct signal is present, and if we reverse the order of the points at  $\phi = 180$  deg, in principle we should reproduce the sequence at  $\phi = 0$  deg exactly, and the difference between the two sequences will be identically zero. However, multipath signals from fixed locations in the chamber do not reverse. To quantify these relations, suppose that the measured signal (either gain or phase)  $S_T$  consists of a direct component  $S_D$  and a multipath component  $S_M$ , and we call the difference of the two sequences  $S_\Delta$ . Then

$$S_{D-180}(-\theta) = S_{D-0}(\theta) \quad (3a)$$

and

$$S_{M-180}(\pm\theta) = S_{M-0}(\pm\theta), \quad (3b)$$

as described above, where the number in the subscript indicates the value of  $\phi$  at which the signal is measured, and  $\theta$  is the azimuth angle. It then follows that

$$S_\Delta(\theta) = S_{T,180}(-\theta) - S_{T,0}(\theta) \quad (4a)$$

or

$$S_\Delta(\theta) = [S_{D,180}(-\theta) + S_{M,180}(-\theta)] - [S_{D,0}(\theta) + S_{M,0}(\theta)] = S_{M,0}(-\theta) - S_{M,0}(\theta). \quad (4b)$$

That is, the difference of the reversed cut at  $\phi = 180$  deg and the forward cut at  $\phi = 0$  deg is twice the odd part of  $S_M$ . Two consequences are apparent:  $S_\Delta$  is insensitive to the even component of  $S_M$  (meaning multipath originating equally from the left and right sides of the AUT, or from directly above or below), and it does not tell us which side of the AUT the odd component is coming from. Still, this method gives us a good idea of the magnitude of the effect.

It is worth noting also that going beyond  $\phi = 180$  deg to compare other cuts 180 deg apart does not add much information to the first comparison, since all the cuts move the antenna horizontally in the chamber and therefore respond to about the same multipath signals.

Figure 9 is a plot of  $S_\Delta$  gain calculated from measurements of the Exelis C146-27-1 antenna during Session 1. The effect is generally less than 0.2 dB out to about 60 deg boresight angle but approaches 1 dB at 90 deg. More interesting to GRASP is Figure 10 showing the corresponding phase multipath. Here again, the effect is relatively small (less than 1 deg) at all frequencies out to about 60 deg azimuth angle, but it increases to about 3 deg at the L2 and L1 frequencies and 90 deg azimuth. Together with the gain plot, this increase suggests the presence of a significant multipath source to either the right or left of the positioner. The phase effect is troubling if GRASP intends to make GNSS measurements much beyond 60 deg boresight angle, because 3 deg corresponds to 1.6 mm at L1.

Figure 11 is a plot of gain data generated in exactly the same way from a scan of the Exelis C146-27-1 antenna during Session 2. Although the antenna and choke ring are slightly

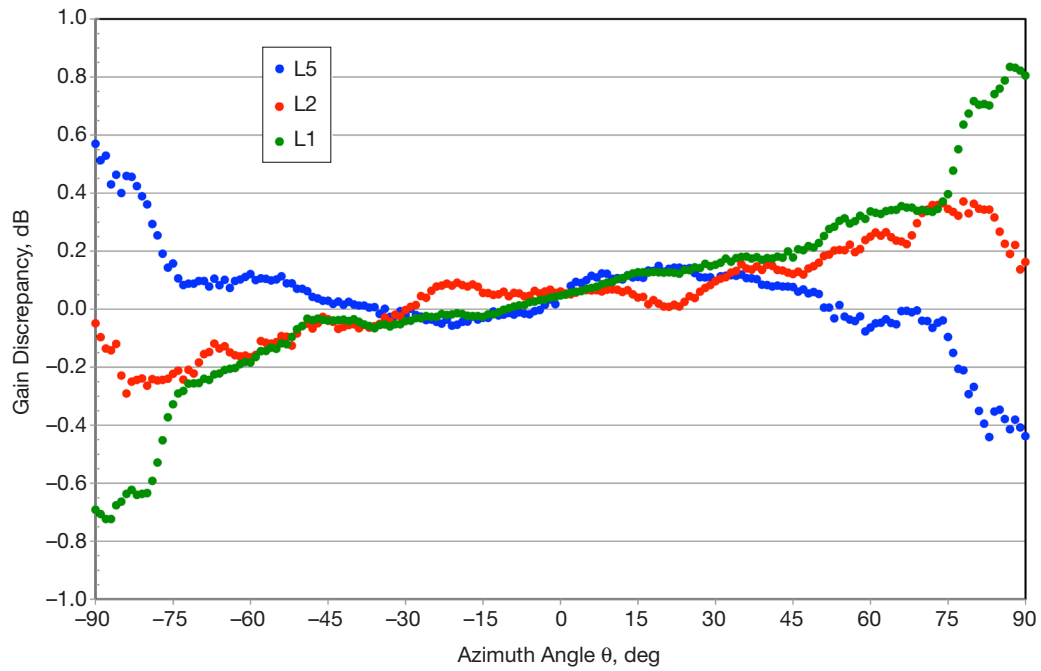


Figure 9. Gain multipath at GEAC from measurements at different orientations, Session 1.

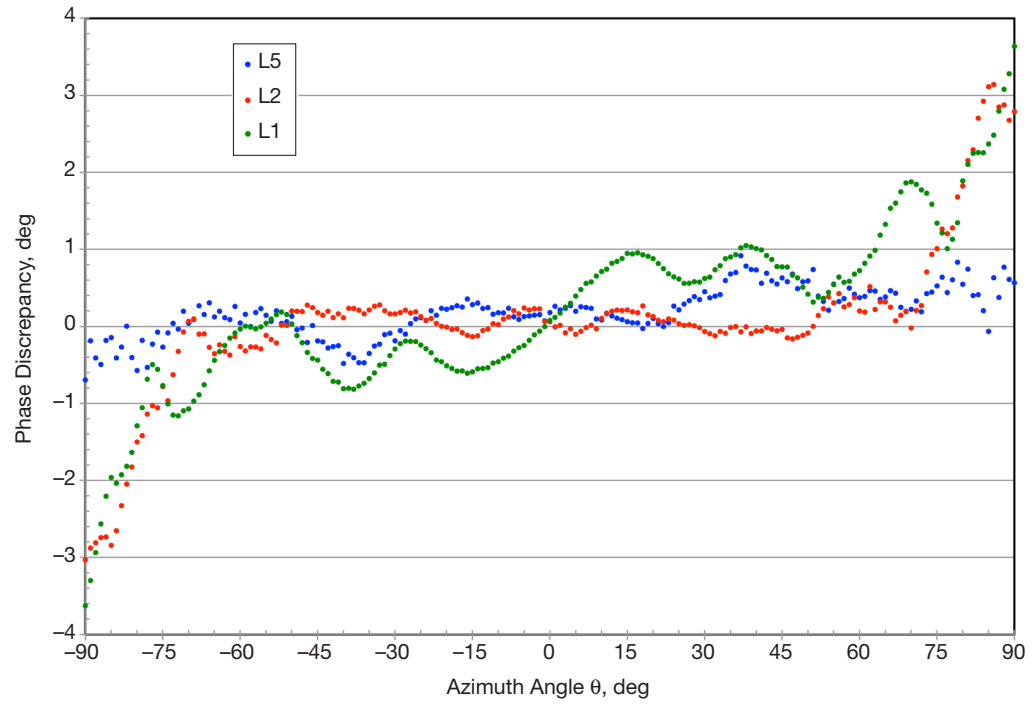


Figure 10. Phase multipath at GEAC from measurements at different orientations, Session 1.

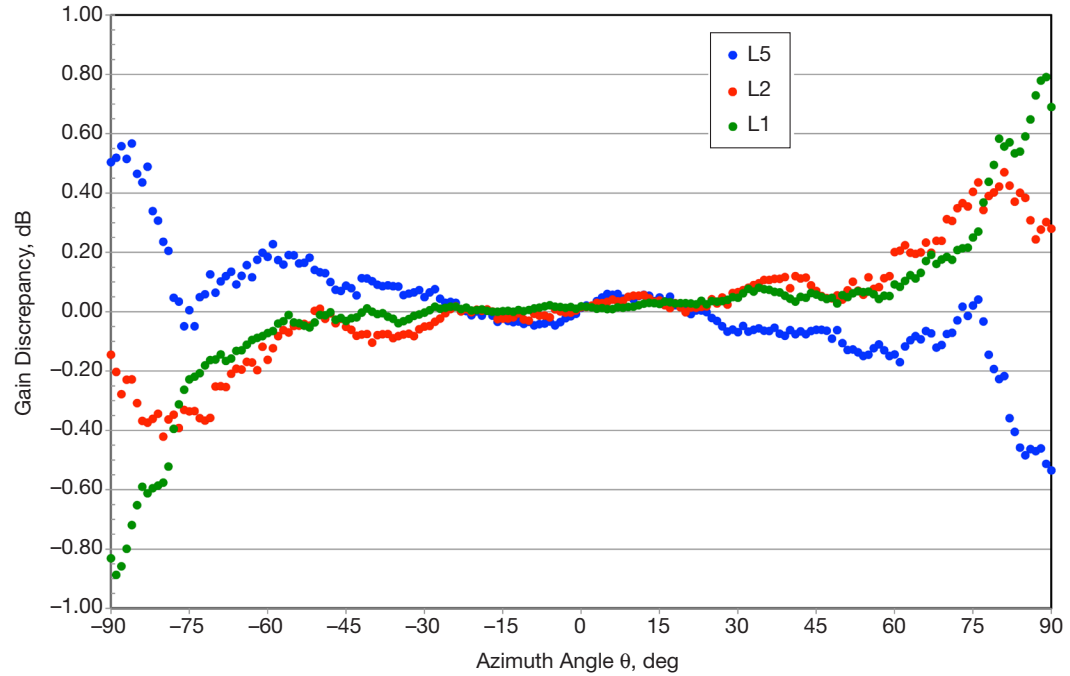
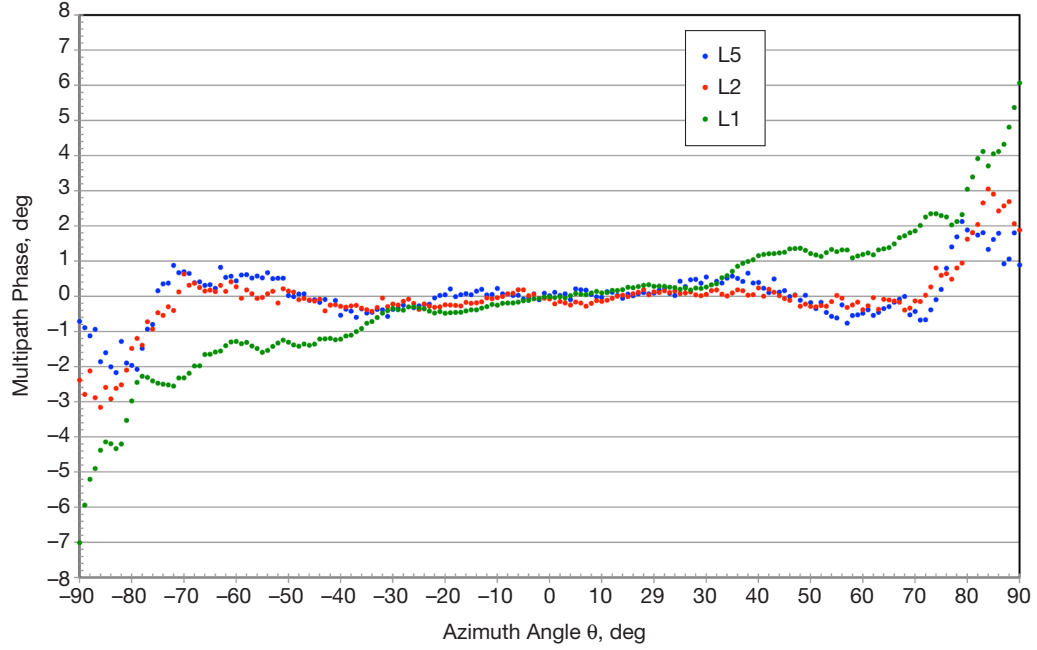


Figure 11. Gain multipath at GEAC from measurements at different orientations, Session 2.

different, the chamber multipath looks virtually the same as Figure 9. The corresponding phase multipath in Figure 12 also resembles that seen in Session 1, although the amplitude of the variation at L1 is somewhat larger.



**Figure 12. Phase multipath at GEAC from measurements at different orientations, Session 2.**

Figures 11 and 12 reinforce the impression that there is a significant multipath source to one side or the other of the positioner. Indeed, we know that there is a door and hardware for a compact chamber on the left that could be the source. From the magnitude of the offsets in the figures, we can estimate how strong that source is relative to the direct signal. In the case of the gain multipath, we have (compare Equation 2)

$$\frac{P_M}{P_D} = 20 \log_{10} (10^{\Delta P/20} - 1), \quad (5a)$$

where  $P_M/P_D$  is the ratio of power in the multipath signal to power in the direct signal, in dB, and  $\Delta P$  is the gain change (considered positive) induced by multipath, in dB.

Estimating from phase,

$$\frac{P_M}{P_D} = 20 \log_{10} \left( \frac{\pi \Delta \phi}{180} \right), \quad (5b)$$

where  $\Delta \phi$  is the phase change caused by the multipath, in degrees.

We want to evaluate the multipath changes at a boresight angle where the supposed multipath source is near the center of the beam, but not so far out that the gain of the direct signal is very weak and unreliable. If we pick about 60 deg and use a rough average of the

three frequencies, then  $\Delta P \approx 0.15$  dB and  $\Delta\phi \approx 1$  deg, leading to  $P_M/P_D \approx -35.1$  dB from the gain equation and  $-35.2$  dB from the phase equation. The agreement is mostly fortuitous, but it does reassure us that we have some idea of what is happening here.

Remember also that  $-35$  dB is the power in the multipath signal relative to the direct signal at 60 deg boresight angle, which is about 8 dB (again, a rough average over the three frequencies) down from the value on boresight. So it looks as though the multipath is actually something like 43 dB below the direct signal — maybe more like 40 dB if we account for the fact that the multipath signal is not on boresight either. This is about the level at which multipath was measured when the range was certified at 1750 MHz.<sup>2</sup>

We also tried to probe multipath in two other ways during Session 2. Both attempts involved the same Exelis POD antenna mounted on the GRACE-FO mockup. Our first strategy was to continue the head angle rotation from 180 deg through 350 deg, measuring each point in the pattern (except the boresight direction) at two different orientations of the boresight. The second strategy was to do a complete scan in the normal configuration, and then repeat the scan with the antenna on a bracket that was 15 cm longer. In this way, each point in the pattern would be measured at two different locations in the chamber separated by 15 cm, and the two sets of results would reflect the different interactions of the direct and reflected signals at the two locations. The strategies were sound, but the execution failed because in both cases the observed multipath came predominantly from the moving mockup rather than the stationary chamber. If we had run the scans without the mockup, they would have given us the information we expected.

## 2. Multipath detection at NSI

Because of the way the data are processed at NSI, we cannot see the effect directly in the reported patterns, as we do at GEAC. But NSI has the MARS software that undertakes to remove the effect of multipath, so we can get an idea of the size of the multipath signal by examining what it does to the data. NSI estimates that at GPS frequencies MARS reduces the effect of multipath from about 30 dB below the direct signal to 50 dB below.<sup>3</sup>

As a typical example, Figure 13 shows the change in gain calculated by MARS at our three frequencies for Scan 1, the simplest configuration, as a function of  $\theta$  for  $\phi = 0$  deg. The other three scans show similar behavior. The maximum correction is something like 0.12 dB, a little less than we see in Figure 11 for GEAC. Equation (5a) then says the multipath signal is 37.1 dB weaker than the direct signal. Figure 14 shows the corresponding differences in phase before and after MARS. Again, the multipath looks a little weaker than at GEAC. If the maximum is 0.7 deg, then Equation (5b) gives a multipath level 38.3 dB below the direct signal, and again the two data types agree rather well. Of course, all these computations are casual and only semi-quantitative, but that is as much as the data really justify. On the whole, NSI looks a little better than GEAC without MARS, and with MARS multipath should not be a concern at all at NSI.

---

<sup>2</sup> Victor Marrero Fontanez, GEAC, personal communication, September 18, 2015.

<sup>3</sup> Pat Pelland, NSI, personal communication, September 17, 2015.

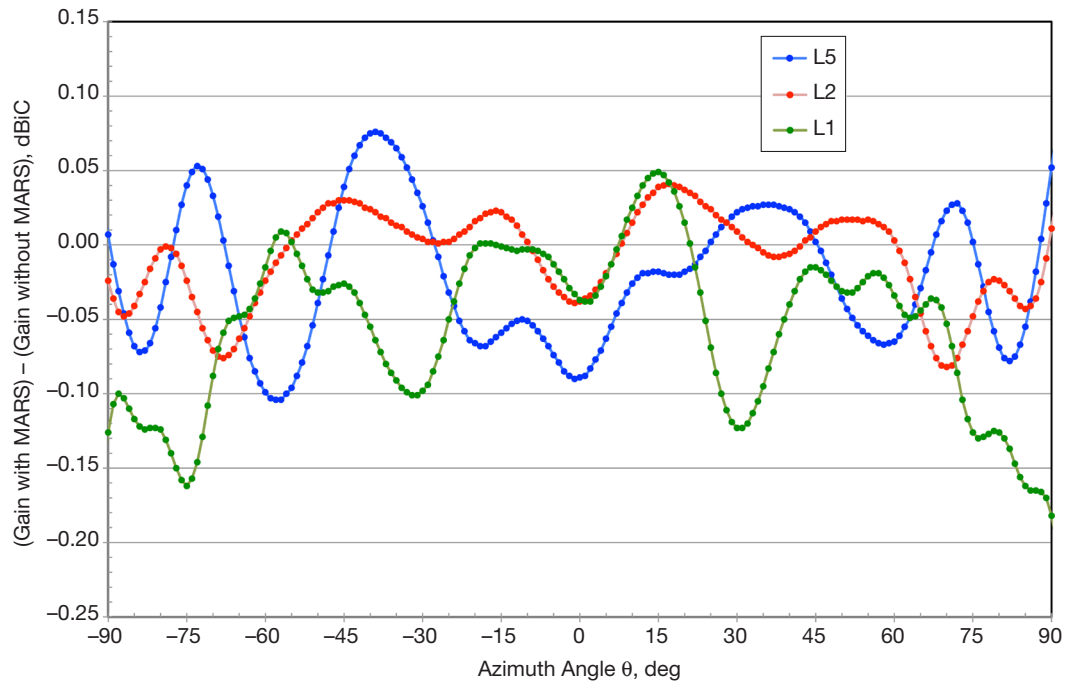


Figure 13. Gain adjustments made by MARS, Scan 1, 0 deg head angle.

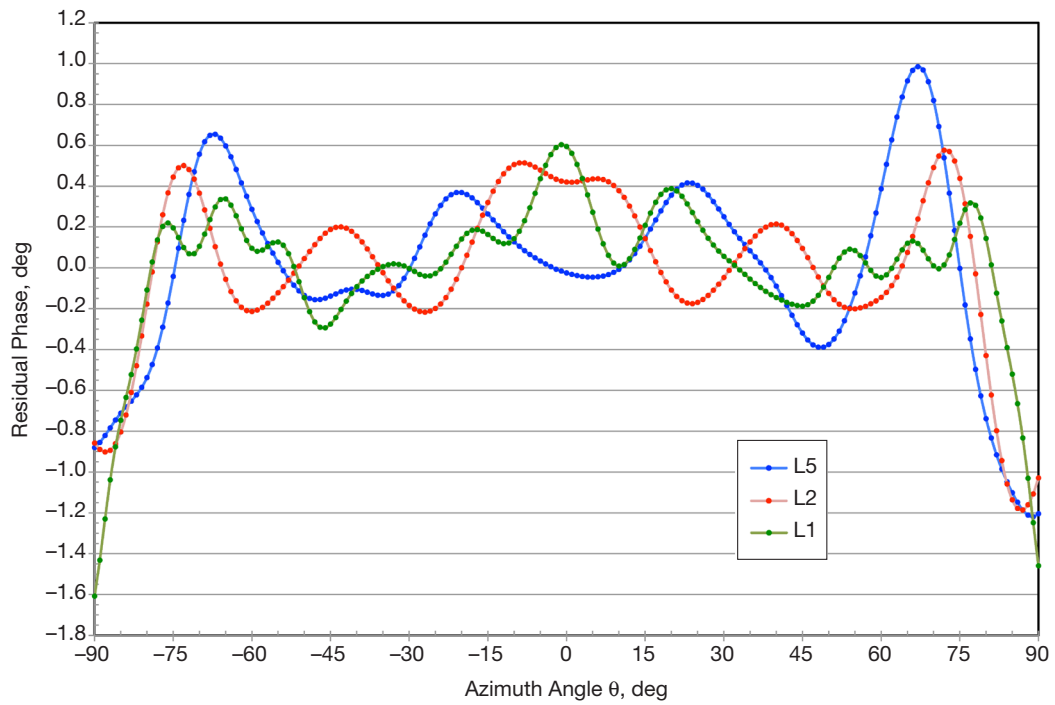


Figure 14. Phase adjustments made by MARS, Scan 1, 0 deg head angle

### C. Direct Comparison of GEAC and NSI Results

Ultimately we can satisfy ourselves that a range is giving GNSS antenna locations accurate to the submillimeter level needed by GRASP only by comparing that range's locations to those measured elsewhere and finding agreement at the required level. Of course, agreement does not prove that the locations are correct, but statistically it constrains the plausible range of error, particularly as the number of ranges increases. For that reason, regardless of the limits we estimate for individual error sources, only direct comparison of the locations computed from the GEAC and NSI measurements can provide convincing evidence that the ranges are performing adequately.

For processing GNSS phase measurements in orbit, the “location” of the antenna on the GRASP spacecraft, to first order, is the computed phase center. However, the effective location of the antenna depends on the direction of the received signal, and the phase center is only a global approximation to that; so more rigorous processing uses an antenna location that combines the phase center with a residual phase that restores the exact antenna phase in the relevant direction. Hence, a proper comparison of GEAC and NSI phase measurements involves both the phase centers and the residual phases. Here we present phase-center results for all three frequencies and all four scans at NSI along with their counterparts at GEAC, and we compare residual phases for one particular case. First, however, we briefly compare gain results at the two chambers.

Figure 15 shows the difference of the NSI (with MARS) and GEAC gains at the three GPS frequencies for NSI Scan 1 (no mockup), and Figure 16 shows Scan 2 (with mockup, star-tracker well covered). Scan 3 closely resembles Scan 2, and Scan 4 is (as expected) practically identical to Scan 1. The comparison before MARS looks much the same. In general, the agreement is remarkable. Chambers generally claim accuracy at the 0.5-dB level, but here the differences do not approach that except at large boresight angles. Incidentally, there is evidence here, especially in Figure 15, that a real difference exists at positive, not negative, azimuth angles. Figures 11 and 12 do not permit that distinction, but this plot more clearly implicates the adjacent compact range at GEAC in the multipath seen there.

Comparing phases at two ranges is harder than comparing gains. Gains fundamentally are what they are and can be compared directly. The pattern of measured phases, however, depends on the three-dimensional offset of the antenna relative to the intersection of the  $\theta$  and  $\phi$  axes of the positioner, and that is inevitably different at different ranges. We can compensate for the difference if we know those relative positions accurately, but we do not know that difference well without computing the location of the phase center (relative to the intersection of axes) at the two ranges. Therefore, that computation needs to precede a detailed comparison of phases and especially phase residuals.

Our phase-center computation is conceptually simple. We begin by assuming that the wavefronts are planar throughout the entire range of motion of the AUT and normal to the  $\phi$  axis of the positioner at  $\theta = 0$  deg. We also impose the convention that the measured phase decreases as the AUT moves away from the chamber antenna that is either transmitting to or receiving from the AUT. The phase model then describes the location of the AUT's phase center as a function of  $\theta$  and  $\phi$  with respect to a chamber coordinate frame

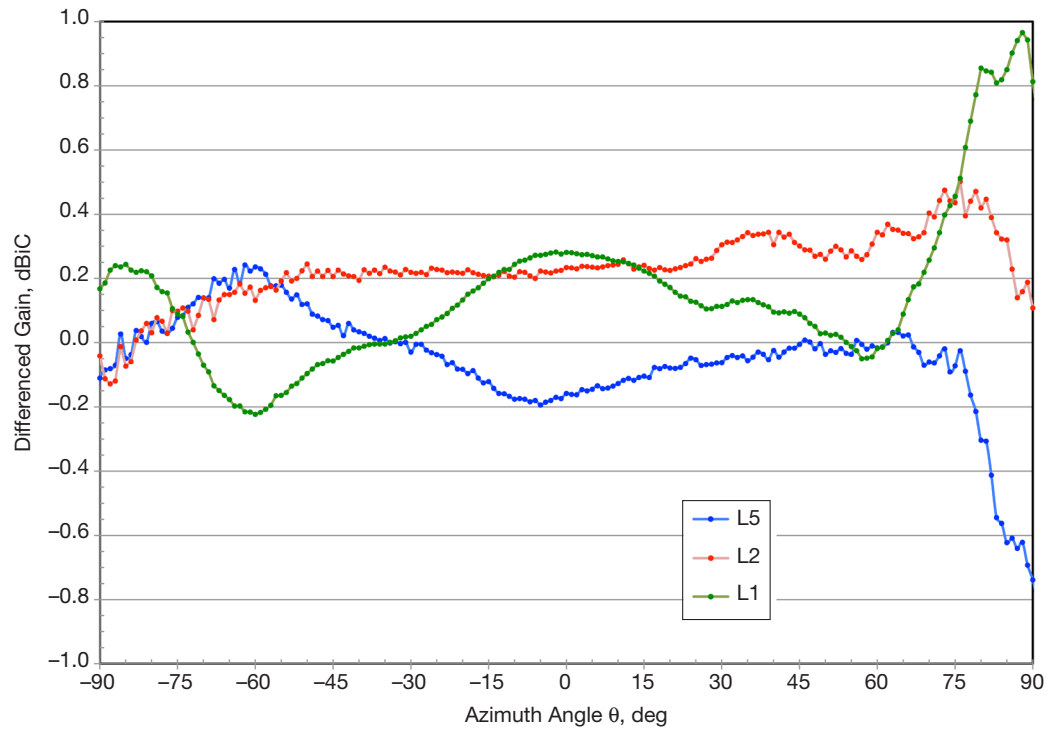


**Figure 15. Difference between gains measured at GEAC and NSI with MARS, Scan 1.**

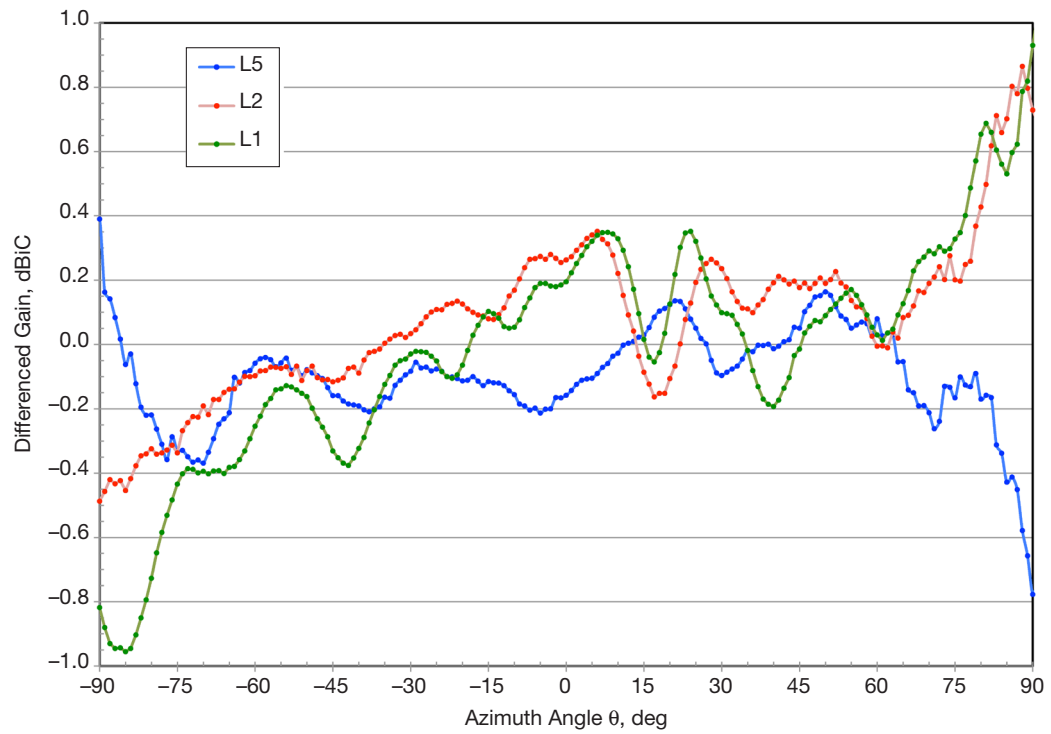


**Figure 16. Difference between gains measured at GEAC and NSI with MARS, Scan 2.**

whose origin is at the intersection of axes. The principal directions are along the  $\theta$  (nominally vertical) axis (the  $z$  coordinate); the  $\phi$  (horizontal) axis,  $y$ ; and  $\hat{x} = \hat{y} \times \hat{z}$  (also horizontal). Unit vector  $\hat{x}$  points to the right as seen from the front (where the chamber antenna is),  $\hat{y}$  points away from the chamber antenna, and  $\hat{z}$  is up, as shown in Figure 17.

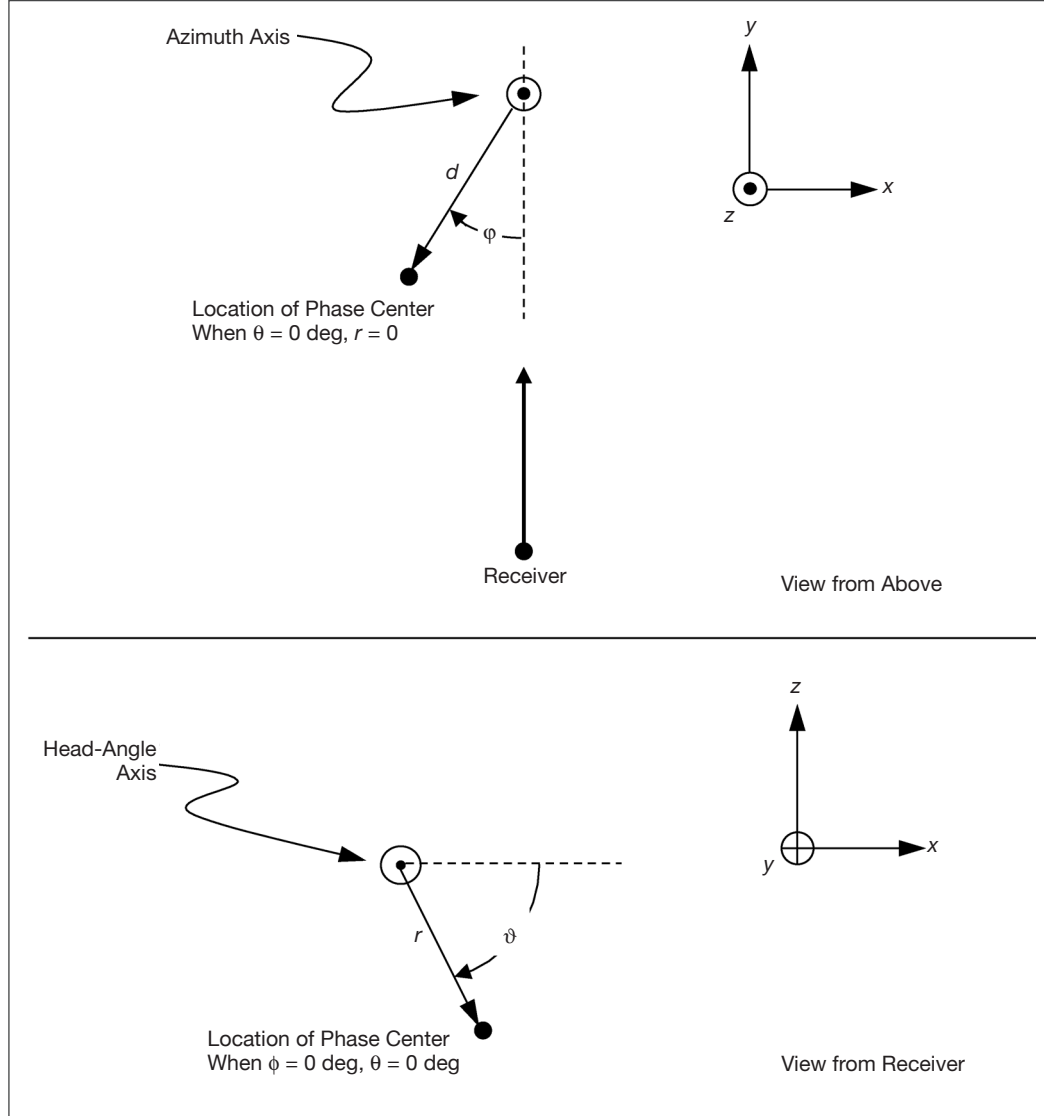


**Figure 17. Geometry of the phase-center model.**

Our phase model then involves five parameters. Parameter  $\zeta_0$  is a global offset equal to the phase that would be measured with the phase center at the origin of coordinates (or anywhere else in the  $x$ - $z$  plane). The remaining parameters are shown in the figure:  $d$  and  $\phi$  are polar coordinates that give the location of the phase center in the  $x$ - $y$  plane if  $r$  is 0. Finally,  $r$  and  $\vartheta$  are polar coordinates that give the location of the phase center relative to the  $\phi$  axis. With  $\theta$  and  $\phi = 0$  deg,  $\vartheta$  increases from 0 deg at the  $+x$  axis, to 90 deg along the  $-z$  axis.

$\zeta_0$  is a nuisance parameter that has no direct bearing on the phase center. For our antennas,  $\varphi$  is either near 0 deg, meaning that the phase center is in front of the intersection of axes, or near  $\pm 180$  deg, meaning that the phase center is behind the intersection of axes; and  $r$  is always on the order of a millimeter or less, generally consistent with the phase center being on the geometric boresight axis, so we do not need to pay much attention to  $r$  and  $\vartheta$ . That leaves  $d$  as our primary interest in comparing solutions.

With the foregoing definitions, the phase model is

$$\zeta = \zeta_0 + d \cos(\theta + \varphi) + r \sin \theta \cos(\phi + \vartheta), \quad (6a)$$

where all the fitting parameters have been defined above.

Equation (6a) can be rewritten as

$$\zeta = \zeta_0 + \zeta_1 \sin \theta + \zeta_2 \cos \theta + \zeta_3 \sin \phi \sin \theta + \zeta_4 \cos \phi \sin \theta, \quad (6b)$$

where  $\zeta_1 = -d \sin \varphi$ ,  $\zeta_2 = d \cos \varphi$ ,  $\zeta_3 = -r \sin \vartheta$ , and  $\zeta_4 = r \cos \vartheta$ , so that the least-squares solution is linear. Then the parameters of interest can easily be computed from the fitting parameters  $\zeta_i$ . Each fit uses the phase data from  $\theta = 0$  deg through 75 deg and  $\phi$  from 0 deg through the largest value less than 180 deg. The data are weighted in proportion to  $\sin \theta$  so that equal solid angles are weighted equally.

These fits give us the locations of the phase centers for the various configurations and frequencies in the chamber frame with its origin at the intersection of the  $\theta$  and  $\phi$  axes of the positioner. For use on the spacecraft, or for comparison of the chambers, we must translate those coordinates to a frame defined with respect to the physical structure of the antenna. In our case, the origin of the antenna frame is the mechanical center of the back surface of the choke ring. Both chambers did surveys to determine the three-dimensional offset between the two frames. GEAC did careful laser measurements at the time of our testing and found the antenna reference point to be 89.2 mm behind the chamber origin, with a negligible component perpendicular to the boresight axis. At NSI, the calculation was slightly more complicated: The plate on their positioner to which our mounting bracket was bolted was 794.44 mm behind the intersection of axes, and our mounting bracket extended 374.86 mm in front of that, for a net offset of 419.58 mm. There again, the offset perpendicular to the boresight axis was negligible.

We applied the chambers' respective offsets to the least-squares phase centers for the four scans at NSI (with and without MARS) and their counterparts at GEAC with the results in Table 8. These offsets affected only the  $d$  parameter (strongly) and the  $\varphi$  parameter (slightly), not  $r$  or  $\vartheta$ .

In the table, we show solutions for GEAC, for NSI without MARS, and for NSI with MARS. Scans 1 and 4 are grouped together for easy comparison because they are nominally identical, and a single scan at GEAC corresponds to both. The  $\varphi$  column is not interesting: All the phases are very close to zero. Likewise, the  $r$ s are all small, and despite some correlations between measurements that hint at real offsets, we do not need to pay much attention to

**Table 8. Estimated phase-center locations in the antenna frame from GEAC and NSI.**

Band	NSI Scan Number	How Measured	$d$ , mm	$\varphi$ , deg	$r$ , mm	$\vartheta$ , deg	RMS Residual, mm
L5	Scan 1	GEAC	107.855	-0.056	0.376	-103.282	1.312
		NSI no MARS	101.999	0.008	0.453	-111.079	1.364
		NSI with MARS	101.344	0.000	0.421	-109.628	1.221
	Scan 4	GEAC	107.855	-0.056	0.376	-103.282	1.312
		NSI no MARS	102.084	-0.007	0.152	-173.815	1.382
		NSI with MARS	101.580	-0.007	0.132	-171.347	1.270
	Scan 2	GEAC	105.948	0.209	0.447	-138.174	1.551
		NSI no MARS	99.609	0.083	0.183	-17.504	1.541
		NSI with MARS	99.645	0.082	0.187	-17.829	1.540
	Scan 3	GEAC	105.252	-0.012	0.262	157.117	1.950
		NSI no MARS	98.924	0.026	0.295	46.148	1.959
		NSI with MARS	98.969	0.026	0.295	45.483	1.962
L2	Scan 1	GEAC	95.320	0.000	0.309	-65.740	1.304
		NSI no MARS	88.675	0.044	0.673	0.673	1.269
		NSI with MARS	88.430	0.043	0.664	-76.845	1.156
	Scan 4	GEAC	95.320	0.000	0.309	-65.740	1.304
		NSI no MARS	88.843	0.025	0.302	-55.948	1.264
		NSI with MARS	88.758	0.026	0.309	-54.918	1.203
	Scan 2	GEAC	91.400	0.144	0.425	-104.050	1.208
		NSI no MARS	85.562	0.096	0.631	-39.708	1.075
		NSI with MARS	85.615	0.101	0.641	-40.187	1.073
	Scan 3	GEAC	91.456	-0.064	0.180	18.461	1.580
		NSI no MARS	85.263	0.042	0.621	-4.744	1.549
		NSI with MARS	85.318	0.043	0.627	-4.983	1.547
L1	Scan 1	GEAC	68.032	0.540	1.125	-67.214	1.934
		NSI no MARS	62.091	0.006	1.113	-80.595	2.068
		NSI with MARS	62.051	0.014	1.127	-81.016	2.022
	Scan 4	GEAC	68.032	0.540	1.125	-67.214	1.934
		NSI no MARS	62.040	0.024	0.872	-72.157	2.046
		NSI with MARS	62.129	0.014	0.845	-71.531	2.030
	Scan 2	GEAC	65.177	0.355	0.608	-103.869	1.294
		NSI no MARS	57.585	-0.068	0.987	-58.709	1.250
		NSI with MARS	57.584	-0.066	0.988	-58.937	1.241
	Scan 3	GEAC	65.685	0.491	0.769	-90.894	1.737
		NSI no MARS	58.192	-0.036	1.029	-59.605	1.715
		NSI with MARS	58.196	-0.036	1.030	-59.548	1.706

$r$  and  $\vartheta$ . The RMS residuals of the fits are interesting, though. On the whole, the residuals at NSI with MARS are about 3 percent smaller than the residuals without MARS and also about 3 percent smaller than the corresponding numbers at GEAC. That suggests that MARS is improving the NSI solutions a little and that NSI is making marginally better measurements than GEAC; but actually the residuals mostly reflect the fact that the single-phase-center model does not fit the data particularly well. If the fit had been extended to

$\theta = 90$  deg, however, the RMS at GEAC would have suffered relative to NSI because of multipath from the compact chamber discussed above.

The most significant phase-center parameter for comparing the two chambers is therefore  $d$ . Considering the 12 independent measurements, the mean offset of the values for NSI with MARS relative to the GEAC values is  $-6.48$  mm with a standard deviation of  $0.58$  mm. If we assume equal variances and independent estimates, that implies that the uncertainty of a single undifferenced estimate of  $d$  is  $0.58/\sqrt{2} = 0.41$  mm, and the uncertainty of the mean offset is  $0.58/\sqrt{12} = 0.17$  mm. This is both good news and bad. The fact that the difference between antenna locations measured at two rather different chambers is consistent to  $0.58$  mm argues that the submillimeter accuracy required by GRASP can be achieved without extraordinary effort. On the other hand, the  $6.5$ -mm offset — much bigger than our measurement uncertainties — implies that we have missed a significant piece of our mechanical calibrations. We have looked hard for this piece and continue to look. Additional measurement of the same configurations at a third chamber may help narrow the search.

Even though the phase-center estimates derived from the measurements at GEAC and NSI agree well, one can argue that for real measurements in orbit the number that matters is the antenna phase in the specific direction of an incoming signal — in other words, the sum of the phase model and the residual phase. It seems reasonable to infer that if the models and the RMS residuals are nearly identical, then the point-by-point residuals must also be nearly the same, but that intuition is easy to test. As an example picked at random, consider Scan 2 at the L2 frequency, and look at  $\phi = 0$  deg. The measurements and models look quite different at the two ranges because of the different geometries, but the residuals are generally the same to within a degree, as shown in Figure 18.

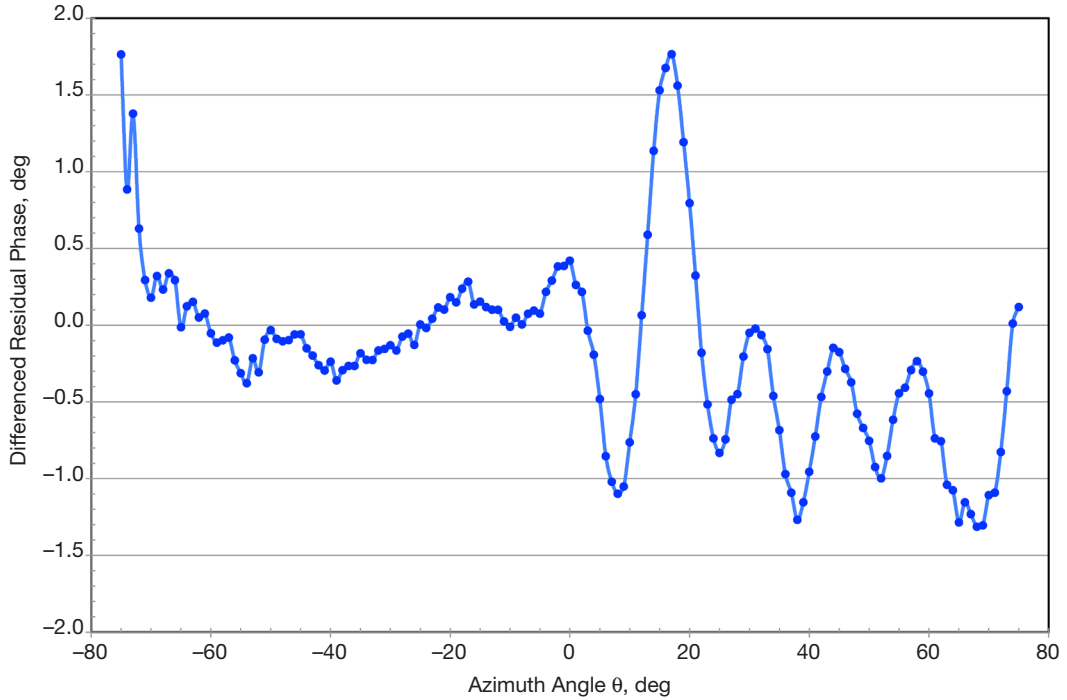


**Figure 18. Difference of residual phases, NSI–GEAC, Scan 2, head angle 0 deg.**

#### **IV. Summary**

The GRASP mission requires relative sensor locations on the GRASP spacecraft accurate to a millimeter or better. For RF sensors like a GNSS receiver, the sensor location is the effective position of the antenna, which is determined by measurements at an antenna test range. Various types of range are available, but accuracy of a millimeter approaches the claimed capability of all of them. To determine whether two rather different facilities agree within the GRASP requirements, we have measured the patterns of typical GNSS spacecraft antennas at both and compared the results. We first measured two Exelis antennas on choke rings in several configurations at the tapered far-field range at Goddard Space Flight Center. Later we duplicated three of those configurations in the spherical near-field range at Nearfield Systems, Inc., in Torrance, California. Together, these measurements enabled us to measure errors caused by thermal noise, remounting of the antennas, instrumental drift, and chamber multipath. Comparison of the Goddard and NSI results also gave a good idea of the total uncertainties in antenna location due to all errors (not just those estimated explicitly).

In general the two ranges performed about equally well. Errors due to thermal noise and remounting of the antennas are generally in the range of a few hundredths of a millimeter on a single measurement point, insignificant in relation to GRASP's requirement. Instrumental drift is observable at Goddard but hidden at NSI. If observed, it can be removed, but the effect of drift on the estimated antenna location at Goddard is less than 0.01 mm even without compensation. Multipath at Goddard appears to be about 40 dB weaker than the direct signal but contributes significant phase error of 2 or 3 deg at boresight angles near 90 deg, apparently because of reflections associated with an adjacent compact range. At NSI, evidence of multipath comes from the adjustments applied by the MARS software, which removes most of the effect. These adjustments indicate a multipath level 37 or 38 dB below the direct signal before MARS, and the level after MARS is probably more than 50 dB below the direct signal.

Direct comparison of locations derived from three GPS frequencies for three different antenna configurations at Goddard and NSI finds a mean offset of 6.48 mm along the antenna boresight axis, but the standard deviation of the twelve measurements is only 0.58 mm, which we believe reflects the true consistency of the two ranges. We suspect that the offset is an error in mechanical calibration and are seeking the cause. Comparison of phase residuals for a particular case from the Goddard and NSI antenna locations shows that total antenna phase agrees at the same level as the phase model.

#### **Acknowledgments**

This investigation would not have been possible without the professional and dedicated work of the personnel at the ranges, particularly Steve Seufert, Victor Marrero Fontanez, and Ken Hersey at Goddard and Pat Pelland at NSI. They conducted the measurements and patiently answered our many questions about details of the ranges. Neil Chamberlain of JPL gave helpful advice throughout the process, especially in his meticulous scrutiny of this article as referee.

## References

- [1] Y. Bar-Sever, B. Haines, W. Bertiger, S. Desai, and S. Wu, "Geodetic Reference Antenna in Space (GRASP) — a Mission to Enhance Space-Based Geodesy," COSPAR Colloquium: Scientific and Fundamental Aspects of the Galileo Program, Padua, Italy, 2009.
- [2] A. C. Newell, "Error Analysis Techniques for Planar Near-Field Measurements," *IEEE Transactions on Antennas and Propagation*, vol. 36, no. 6, pp. 754–768, June 1988.
- [3] G. Hindman and A. C. Newell, "Mathematical Absorber Reflection Suppression (MARS) for Anechoic Chamber Evaluation & Improvement," Antenna Measurement Techniques Association Annual Meeting and Symposium, Boston, Massachusetts, November 20, 2008.